BIOCHEMISTRY
including biophysical chemistry & molecular biology

Article

pubs.acs.org/biochemistry

Single Mutation Alters the Substrate Specificity of L-Amino Acid Ligase

Takeo Tsuda,* Mana Asami, Yoshiaki Koguchi, and Shuichi Kojima

Department of Life Science, Faculty of Science, Gakushuin University, 1-5-1 Mejiro, Toshima-ku, Tokyo 171-8588, Japan

Supporting Information

ABSTRACT: L-Amino acid ligase (Lal) catalyzes the formation of a dipeptide from two L-amino acids in an ATP-dependent manner and belongs to the ATP-grasp superfamily. *Bacillus subtilis* YwfE, the first identified Lal, produces the dipeptide antibiotic bacilysin, which consists of L-Ala and L-anticapsin. Its substrate specificity is restricted to smaller amino acids such as L-Ala for the N-terminal end of the dipeptide, whereas a wide range of hydrophobic amino acids including L-Phe and L-Met are recognized for the C-terminal end *in vitro*. We determined the crystal structures of YwfE with bound ADP-Mg^{2+}-Pi and ADP-Mg^{2+}-L-Ala at 1.9 and 2.0 Å resolutions, respectively. On the basis of these structures, we generated point mutants of residues that are considered to participate in the recognition of L-Ala and measured their ATPase activity. The conserved Arg328 is suggested to be a crucial residue for L-Ala recognition and catalysis. The mutation of Trp332 to Ala caused the enzyme to hydrolyze ATP, even in the absence of L-Ala, and the structure of this mutant protein appeared to show a cavity in the N-terminal substrate-binding pocket. These results suggest that Trp332 plays a key role in restricting the substrate specificity to smaller amino acids such as L-Ala. Moreover, Trp332 mutants can alter the substrate specificity and activity depending on the size and shape of substituted amino acids. These observations provide sufficient scope for the rational design of Lal to produce desirable dipeptides. We propose that the positioning of the conserved Arg residue in Lal is important for enantioselective recognition of L-amino acids.

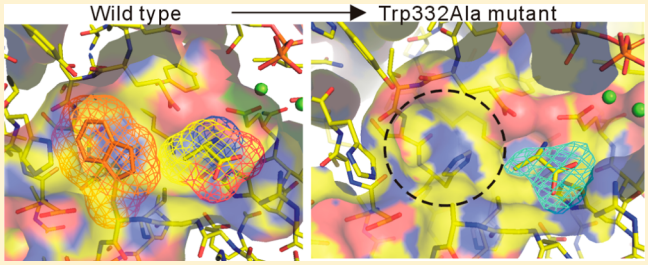

Microorganisms produce a wide range of biologically active peptide compounds such as antibiotics, antitumors, and siderophores.[1] Most of these compounds are produced via two distinct biosynthetic strategies. The first strategy uses ribosomal synthesis of linear precursor peptides that undergo posttranslational modification and proteolysis.[2] The second strategy uses nonribosomal peptide synthetase (NRPS), a large enzyme composed of multiple modules.[3,4] Independent of these two pathways, several L-amino acid ligases (Lals), which are enzymes catalyzing the ATP-dependent formation of an α-peptide bond between two L-amino acids, have been identified in certain microorganisms.[5−8] For example, *Bacillus subtilis* YwfE (also referred to as BacD), the first identified and well-studied Lal,[5] produces a dipeptide antibiotic called bacilysin that consists of L-Ala at the N-terminus and the nonproteogenic amino acid, L-anticapsin, at the C-terminus[9] (Scheme 1). The substrate specificity of YwfE is restricted to smaller amino acids such as L-Ala, for the N-terminal end of the dipeptide, whereas a wide range of hydrophobic amino acids, such as L-Phe and L-Met, are recognized for the C-terminal end. Despite the recognition of a nonproteogenic L-amino acid as a substrate by YwfE, this enzyme is not able to synthesize D-amino acid-containing dipeptides (Scheme 1).

Lal belongs to the ATP-grasp superfamily of enzymes, which catalyze the formation of an amide bond between a carboxylate compound and an amine compound in an ATP-dependent manner.[10,11] ATP-grasp enzymes share a similar overall fold composed of three domains (A, B, and C) and similar binding modes for nucleotides. However, they accept a wide range of carboxylate and amine substrates, and the sequence and structural conservation of the binding sites for these substrates is much lower. The catalytic mechanism of the enzymes in this superfamily is considered to involve the initial activation of the carboxyl group of a substrate by ATP-phosphorylation to form an acylphosphate intermediate. This is followed by a nucleophilic attack by the amine group of a second substrate on the acylphosphate to yield a tetrahedral transition state and the release of phosphate by the tetrahedral intermediate to yield a product.

Scheme 1

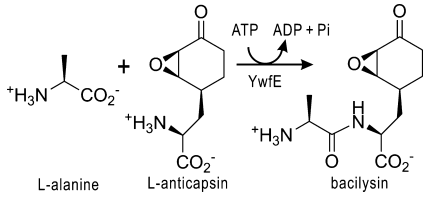

Received: January 22, 2014
Revised: April 4, 2014
Published: April 4, 2014

   dx.doi.org/10.1021/bi500292b | *Biochemistry* 2014, 53, 2650−2660

Some of the ATP-grasp enzymes are considered to be important targets for the development of new antibacterial drugs because of the critical nature of these enzymes and lack of human orthologues. Although Lal is not a clinical target, it has the potential to become an interesting target for the industrial production of useful dipeptides. Dipeptides have unique physicochemical properties and physiological functions. For example, the artificial sweetener aspartame is L-aspartyl-L-phenylalanine methyl ester (L-Asp-L-Phe-OMe). L-Ala-L-Gln is used as a component of patient infusions because of its higher solubility than L-Gln. L-Asp-L-Phe, a precursor of aspartame, was biosynthesized by hybrid NRPS; however, the turnover rate was extremely low (0.7 min^{-1}).[12] Compared with the NRPS system, Lal is a smaller soluble enzyme and participates in a simpler reaction to combine two amino acids. An L-Ala-L-Gln has reportedly been produced via fermentative processes using YwfE-transformed bacteria.[13] However, biochemical and structural studies of Lal are extremely limited compared with those of other members of the ATP-grasp superfamily.

The crystal structures of two Lals have recently been reported. The first determined structure was that of YwfE with bound ADP and phosphinophosphate analogue (P-analogue), which was believed to mimic the tetrahedral transition state.[14] The structure showed that YwfE binds the dipeptide in the reverse orientation to that observed in Ddl, suggesting that the substrate entry mode differs between them. The other structure was BL00235 from *Bacillus licheniformis*, which was bound to ADP and Ca^{2+} ions.[15]

Here, we describe new YwfE crystal structures with bound ADP-Mg^{2+}-Pi and ADP-Mg^{2+}-L-Ala that are refined to 1.9 and 2.0 Å resolutions, respectively. The results suggest that Trp332 plays a key role in N-terminal substrate specificity for smaller amino acids such as L-Ala. Substitution with other residues at position 332 altered the substrate specificity depending on the size and shape of the incorporated residues. These observations afford the possibility of a rational design of YwfE for the production of desirable dipeptides. Furthermore, we propose that based on a structural comparison between Lal and Ddl, the positioning of Arg328 is important for enantioselective recognition of L-amino acids.

EXPERIMENTAL PROCEDURES

Protein Preparation. Cloning, expression, and purification of *Bacillus subtilis* YwfE were performed as previously described,[16] with slight modifications. The gene encoding the full-length protein (Met1−Val472) and deletion mutant (Lys4−Tyr468) of YwfE were amplified using PCR from *B. subtilis* genomic DNA. The amplified PCR products were cloned into the pGEX-6P-1 expression vector (GE Healthcare) with *Bam*HI and *Xho*I sites to produce the fusion protein with N-terminal GST. Mutations were introduced according to the QuikChange site-directed mutagenesis procedure using oligonucleotide primers, except that KODplus (TOYOBO) polymerase was used for PCR. The DNA sequence of the expression plasmid was confirmed by automated DNA sequencing.

The *Escherichia coli* strain ArcticExpress RIL cells (DE3) (Stratagene), containing the expression plasmid, were grown at 37 °C in a Luria−Bertani medium containing 50 μg/mL ampicillin. When the optical density at 600 nm of the culture reached approximately 0.8, expression was induced by the addition of isopropyl β-D-thiogalactopyranoside to a final concentration of 0.3 mM. After an 18-h cultivation at 25 °C, the cells were harvested by centrifugation and suspended in phosphate-buffered saline (PBS) containing 1 mM dithiothreitol (DTT) and lysed by sonication. The lysate was centrifuged at 10,000*g* for 20 min, and the supernatant was loaded onto a Glutathione Sepharose FF column (GE Healthcare) preequilibrated with PBS containing 1 mM DTT. The GST-fused YwfE was eluted with 50 mM Tris-HCl (pH 8.0), 50 mM NaCl, 1 mM DTT, and 15 mM reduced glutathione. The GST tag was cleaved using PreScission protease (GE Healthcare), and the reduced glutathione was removed by extensive dialysis against 50 mM Tris-HCl (pH 8.0), 50 mM NaCl, 1 mM EDTA, and 1 mM DTT. Furthermore, the cleaved GST tag was subsequently removed by chromatography on a Glutathione Sepharose FF column (GE Healthcare). After concentration by ultrafiltration using a Vivaspin-20 10,000 MWCO (Sartorius), the flow-through fraction was loaded onto a HiLoad 16/60 Superdex 75 pg column (GE Healthcare) preequilibrated with 50 mM Tris-HCl (pH 8.0) and 100 mM NaCl. Fractions containing pure YwfE were pooled and dialyzed against 10 mM Tris-HCl (pH 8.0) containing 1 mM DTT and concentrated to approximately 20 mg/mL by ultrafiltration using a Vivaspin-20 10,000 MWCO (Sartorius). The protein concentration was determined by the BCA method (Pierce) using bovine serum albumin as a standard.

Crystallization and Data Collection. Crystallization screening was performed by the hanging-drop vapor-diffusion method at 20 °C.[16] Drops were prepared by manually mixing 2 μL of deletion mutant (Lys4−Tyr468) of YwfE protein solution (8 mg/mL) containing 10 mM ADP, 10 mM $MgCl_2$ (or 5 mM $MnCl_2$), and 10 mM sodium phosphate (pH 7.4) and 2 μL of reservoir solution containing 16%−18% (w/v) PEG 3350, 0.3 M NaCl, 0.1 M HEPES-NaOH (pH 7.0−7.25), 5% (v/v) ethylene glycol, and 1 mM DTT and were equilibrated against 500 μL of reservoir solution. Crystals of the complex with ADP-Mg^{2+}-L-Ala were grown using the same method except that 100 mM L-Ala was added instead of sodium phosphate. The crystallization conditions of the W332A mutant (Lys4−Tyr468) were the same as those for the wild type.

Diffraction data were collected at the BL5A, AR-NE3A, and AR-NW12A beamlines at the Photon Factory (PF; Tsukuba, Japan). Ethylene glycol (20%, v/v) was used as a cryoprotectant for data collection under cryogenic conditions. The crystals were soaked in cryoprotectant-containing mother liquor and flash-cooled in nitrogen stream at 100 K. Mn^{2+}-anomalous data of the Mn^{2+}-derivative crystals were collected at a wavelength of 1.2 Å. The diffraction data sets were processed using the HKL2000 program.[17] All of the crystals belonged to the space group $P6_522$, with one molecule in the asymmetric unit.

Structure Determination and Refinement. Preparation of the SeMet-labeled crystals and data collection using a single-wavelength anomalous dispersion (SAD) method were previously described.[16] To determine the structure of YwfE, SAD phasing, density modification, and automatic model building were performed at 2.8 Å using the CRANK program[18] from CCP4.[19] All of the eight selenomethionine sites in the asymmetric unit were identified with sufficient quality. An initial solvent-flattened electron density map for the polyalanine chains was modeled with the automated model building program ARP/wARP,[20] followed by manual fitting using Coot.[21] Refinement was performed by alternating cycles of manual rebuilding using Coot and refinement using CNS[22] and Refmac5 including TLS refinement.[23] All crystal structures were determined starting from the atomic model obtained

dx.doi.org/10.1021/bi500292b | *Biochemistry* 2014, 53, 2650−2660

Table 1. Diffraction Data and Refinement Statistics of YwfE Crystals[a]

crystal	wild-type ADP-Mg^{2+}-Pi	wild-type ADP-Mg^{2+}-L-Ala	W332A mutant ADP-Mg^{2+}-L-Ala
wavelength (Å)	1.000	1.000	1.000
beamline	PF BL-5A	PF AR-NW12A	PF AR-NW12A
space group	$P6_522$	$P6_522$	$P6_522$
cell $a = b$ (Å)	90.58	90.02	91.13
c (Å)	252.65	249.80	258.76
resolution (Å)	20−1.9 (1.95−1.90)	20−2.0 (2.05−2.00)	20−2.30 (2.35−2.30)
completeness (%)	88.9 (96.5)	98.3 (99.4)	98.1 (100.0)
redundancy	10.6 (11.1)	9.0 (9.3)	7.6 (7.7)
I/σ (I)	53.5 (9.9)	53.5 (8.3)	55.6 (7.6)
R_{merge} (%)	0.069 (0.312)	0.068 (0.350)	0.038 (0.322)
resolution (Å)	20−1.9	20−2.0	20−2.3
number of reflections	41 606	38 656	24 089
R_{work}/R_{free} (%)	19.90/24.30	19.74/23.59	22.36/26.14
number of atoms	4056	3872	3745
protein	3626	3626	3623
ligands	34	35	35
water	396	211	87
overall B-factor (Å^2)	49.6	47.0	73.9
protein	49.7	47.4	74.3
ligands	43.1	42.2	93.6
water	49.2	40.7	51.3
rmsd			
bond lengths (Å)	0.012	0.011	0.011
bond angles (deg)	1.3	1.3	1.3
Ramachandran[b] (%)	90.1/9.7/0.2/0	89.4/10.4/0.2/0	88.0/12.0/0/0
PDB code	3WNZ	3WO0	3WO1

[a]Values in parentheses are for the highest-resolution shells. [b]Fractions of residues in most favored/additionally allowed/generously allowed/outliners of the Ramachandran plot according to Procheck[24] in the CCP4 suite.[19]

using the SAD data set. Procheck[24] was used for Ramachandran analysis. Statistics of the diffraction data and refinement are listed in Table 1 and Supporting Information, Table S1. All protein structure figures were prepared using PyMol.[25]

Measurement of ATPase Activity. ATPase activities of wild-type and mutated YwfE were measured using the Fiske−Subbarow method[26] to colorimetrically quantify the liberated Pi. Standard ATPase assays were performed at 37 °C in 100 μL of the assay buffer containing 10 mM L-Ala; 30 mM L-Phe (or 50 mM L-Met); 100 mM Bicine-NaOH (pH 9.0); 10 mM $MgCl_2$; 10 mM ATP; and 2.5, 5.0, 7.25, 10, or 15 μg/mL purified full-length YwfE in a 96-well assay plate. Reaction times (between 10 and 45 min) and concentrations of protein (between 2.5 μg/mL and 15 μg/mL) used in the assay were varied depending on the degree of activity. Reactions were started by the addition of 10 μL of 100 mM ATP and stopped by the addition of 50 μL of stop solution containing 10% TCA and 0.1% SDS. Furthermore, 100 μL of the molybdate solution (0.75% ammonium molybdate in 0.675 M H_2SO_4) followed by 10 μL of reducing solution (0.1% 1-amino-2-naphthol-4-sulfonic acid, 1.2% $NaHSO_3$, and 1.2% Na_2SO_3) were added and incubated at 37 °C for 10 min. The amount of released Pi was determined by measuring absorbance at 665 nm using a BiotracII plate reader (GE Healthcare) in a 96-well format. The absorbance of a blank, measured in the condition without protein, was subtracted. Each ATPase activity of the wild-type protein in the presence of 10 mM L-Ala or 30 mM L-Phe alone exhibited activity similar to the background. Pi standards were prepared by dissolving KH_2PO_4 in the buffer. To determine the kinetic parameters, the velocity versus substrate concentration data were subjected to nonlinear least-squares analysis using the Michaelis−Menten equation, $v = V_{max}[S]/([S] + K_m)$, using the SigmaPlot software. All data are presented as the mean ± standard deviation of at least three independent experiments.

Analysis of Dipeptide by HPLC. The reactions were performed at 37 °C in 500 μL of the assay buffer containing 50 mM L-Phe; 100 mM Bicine-NaOH (pH 9.0); 10 mM $MgCl_2$; 10 mM ATP; and 10 μg of purified full-length W332A mutant. After an 18-h incubation, the reactions were stopped by the addition of 0.1% trifluoroacetic acid, and 250 μL of the reaction mixtures were subjected to a reverse-phase HPLC (C_{18} column: 250 mm × 4.6 mm; Kaseisorb LC ODS-120−5, Tokyo Chemical Industry, Japan) with a gradient of acetonitrile in 0.1% trifluoroacetic acid at a flow rate of 0.8 mL/min (elution program: 0 to 15 min, 0% of CH_3CN; 15 to 39 min, a linear increase in CH_3CN from 0% to 32%; 39 to 40 min, a linear increase in CH_3CN from 32% to 80%). Absorbance was monitored at 230 nm. An authentic sample of L-Phe-L-Phe (Sigma-Aldrich) was used as a standard.

RESULTS AND DISCUSSION

Crystal Structures of YwfE in Complex with ADP-Mg^{2+}-Pi and ADP-Mg^{2+}-L-Ala. To elucidate the substrate binding mode and reaction mechanism of L-amino acid ligase (Lal), we prepared native and Se-Met derivative crystals of *B. subtilis* YwfE in the presence of ADP, Mg^{2+}, and L-Ala-L-Gln dipeptide.[16] Although no electron density corresponding to the dipeptide was observed, an unexplained tetrahedral-shaped piece of weak electron density appeared over the β-phosphate group of bound ADP. We assumed this to be an inorganic

dx.doi.org/10.1021/bi500292b | Biochemistry 2014, 53, 2650−2660

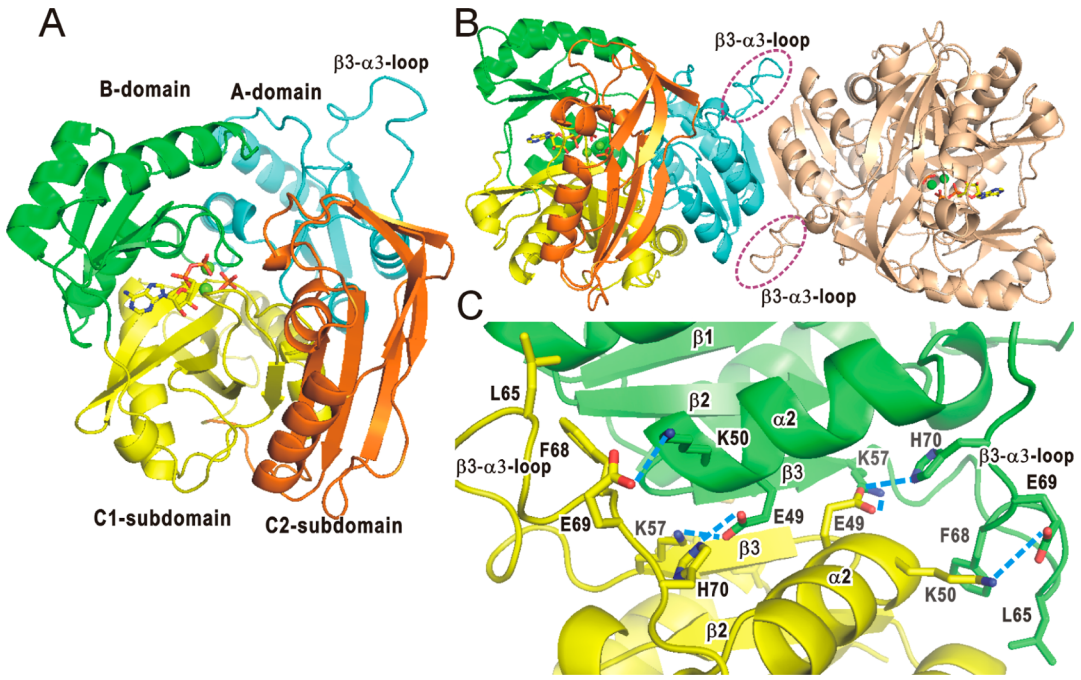

Figure 1. Crystal structure of YwfE from *Bacillus subtilis*. (A) Overall structure of YwfE with bound ADP-Mg^{2+}-Pi. ADP and Pi molecules are presented as a stick model. Two Mg^{2+} ions are presented as green spheres. (B) Oligomeric state of YwfE with bound ADP-Mg^{2+}-Pi. The purple broken circles represent the extended loop region in the A-domain. (C) Close up view of the dimer interface. Two protomers are colored yellow and green. Side chains involved in important interactions in the dimer interface are presented as stick models. The blue broken lines represent the electrostatic interactions between protomers. The figure was prepared using PyMol.[25]

phosphate ion (Pi), which may possibly be derived from the purification procedure. To obtain clear electron density, we attempted to crystallize YwfE in the presence of ADP, Mg^{2+}, and Pi instead of L-Ala-L-Gln. The structure of YwfE with bound ADP, Mg^{2+}, and Pi was determined and refined to 1.9 Å resolution (Table 1). In addition, we determined the structure of YwfE with bound ADP, Mg^{2+}, and L-Ala at 2.0 Å resolution. However, we have not yet determined the crystal structure with bound L-Ala-L-Gln. The YwfE protein used in this study consists of residues Lys4−Tyr468, which lack the N- and C-terminal short regions, so as to improve the quality of crystals, as previously reported.[16] The overall structure consists of three large A-, B-, and C-domains from the N terminus, and the C-domain is further divided into C1- and C2-subdomains flanked by a large antiparallel β-sheet (Figure 1A). The two structures with ADP, Mg^{2+}, and Pi or L-Ala were extremely similar, with a root-mean-square deviation (rmsd) of 0.23 Å for all Cα atoms. These structures were similar to those of the earlier full-length YwfE (Glu2−Val472) with bound ADP and phosphorylated phosphinate L-Ala-L-Phe analogue (P-analogue)[14] with an rmsd of 0.48 Å for 464 Cα atoms, indicating that the deletion of short peptides at both termini exerts little influence on the overall fold. Moreover, the present structures were similar to another available structure of Lal, BL00235, from *B. licheniformis*[15] with an rmsd of 2.75 Å for 365 structurally equivalent Cα atoms.

Size exclusion gel filtration analysis under low ionic strength conditions has shown dimer formation of YwfE in a solution,[16] and two protomers in the crystals formed a dimer through a crystallographic 2-fold axis (Figure 1B). Because the buried surface area of the dimer interface was calculated to cover only 6% of the total surface of the protomers, either protomer was tightly connected by extension of the central β-sheet over the adjacent protomer in the A-domain (Figure 1C). In addition, the interface was stabilized by electrostatic and hydrophobic interactions of several residues in the α2-helix, the β3-strand, and the extended loop between the β3-strand and α3-helix. This type of β-strand-mediated dimer interaction was observed in the human, yeast, and *Trypansoma brucei* glutathione synthetase (GS) structures, which belong to the ATP-grasp superfamily.[27−29] The dimer interface of *T. brucei* GS was calculated to cover 7.5% of the total surface area of a protomer.[29]

Active Site Structures of YwfE. A Fourier difference ($|F_{obs}| - |F_{calc}|$) map before the introduction of ADP, Mg^{2+}, and Pi into the atomic model clearly showed the bound nucleotide in the cleft between the B-domain and C1-subdomain (Figure 2A). ADP is recognized by conserved residues in a manner similar to that observed in other ATP-grasp enzymes. To confirm the location and number of bound Mg^{2+} ion(s), an Mn^{2+} derivative was prepared by cocrystallization with $MnCl_2$ instead of $MgCl_2$ (Table S1, Supporting Information). An anomalous Fourier map clearly showed the location of two Mn^{2+} beside the β-phosphate group of ADP. Therefore, we modeled two Mg^{2+} ions in the ADP-Mg^{2+}-Pi-bound structure. One of the Mg^{2+} ions labeled "Mg1" in Figure 2 is coordinated by oxygen atoms of the α- and β-phosphate groups of ADP, Glu311, Glu324, Pi, and one water molecule (Figure 2B and C). The other Mg^{2+} labeled "Mg2" in Figure 2 is coordinated by oxygen atoms of the β-phosphate group of ADP, Glu324, Pi, and two water molecules. The bidentate carboxyl group of Glu324, which is the highly conserved residue in ATP-grasp enzymes, bridges two Mg^{2+} ions, suggesting that it plays a crucial role in catalysis. For both Mg^{2+} ions, the metal−ligand distances range from 1.8 and 2.4 Å. In the ADP-Mg^{2+}-L-Ala-bound structure, the location and number of bound Mg^{2+} ions were also confirmed by the Mn^{2+} derivative. Two Mg^{2+} ions are octahedrally coordinated by the same ligands as observed in the

dx.doi.org/10.1021/bi500292b | *Biochemistry* 2014, 53, 2650−2660

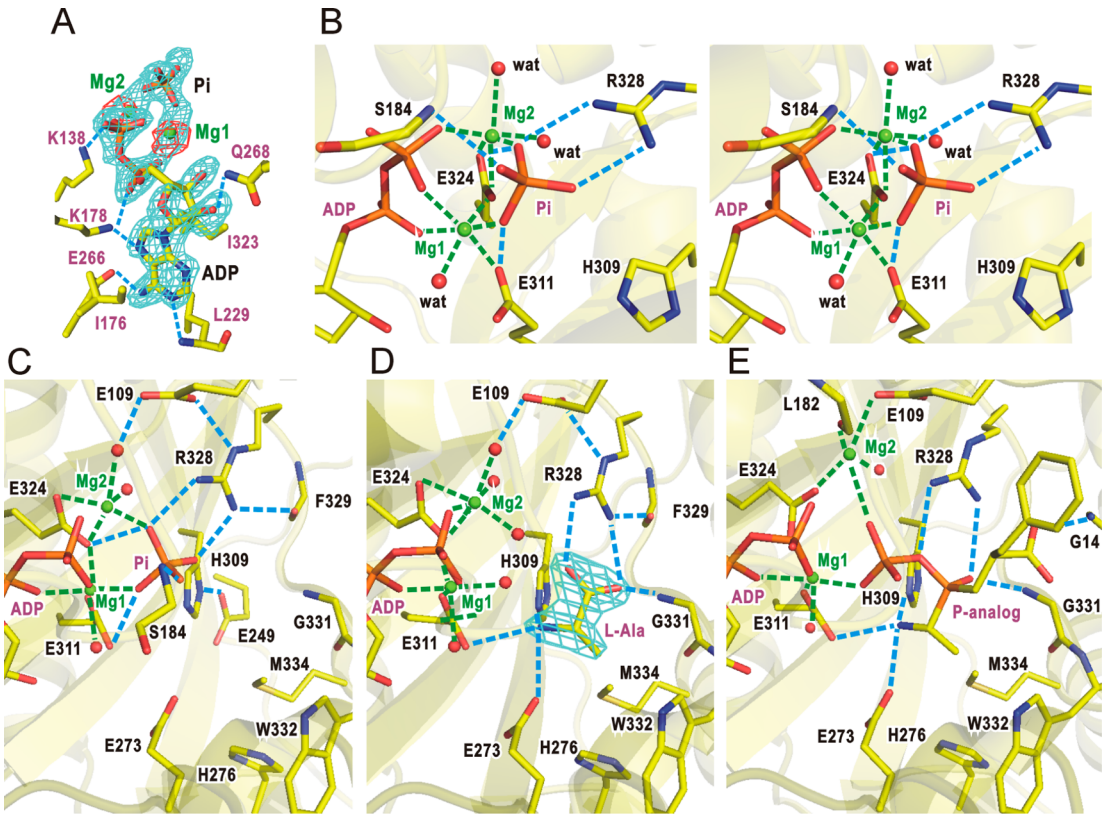

Figure 2. Details of the ligand-binding sites of YwfE. (A) Side chains important for ligand binding are presented as stick models. The cyan net represents a simulated omit map contoured at 2.5σ of ADP-Mg^{2+}-Pi. The red net represents an anomalous Fourier difference map for Mn^{2+} of ADP-Mn^{2+}-Pi-bound form contoured at 10σ. Two Mg^{2+} ions are labeled with Mg1 and Mg2. The blue broken lines represent hydrogen bonds. (B) Stereo view of the Mg^{2+}-Pi-binding site. The red spheres represent Mg^{2+}-coordinating water molecules. The green broken lines represent the coordination of Mg^{2+} ions. The close-up views of (C) ADP-Mg^{2+}-Pi-; (D) ADP-Mg^{2+}-Ala-; and (E) ADP-Mg^{2+}-P-analogue (PDB entry 3VMM)-bound structures are shown in the same view. The cyan net in D represents a simulated omit map contoured at 5σ of L-Ala.

ADP-Mg^{2+}-Pi-bound structure except for substitution of oxygen atoms from a water molecule with those from Pi (Figure 2C). In contrast, in the earlier P-analogue-bound YwfE structure, Mg2 was located at a different position and coordinated by the main-chain carbonyl group of Leu182 and the side chain of Glu109[14] (Figure 2E). A water molecule occupied the same position in our structure (Figure 2C and D). In addition, it should be noted that the present structure showed the side chain of Tyr75 pointed on the opposite side into the active site, although the earlier study suggested that Tyr75 may function as a catalytic base for the deprotonation of the amino group of L-anticapsin, which is a physiological C-terminal end substrate of YwfE[14] (Figure S1, Supporting Information).

The bound Pi is stabilized by hydrogen bonds with the main-chain amide group of Ser184 in the B-domain and the side chains of Glu311, Glu324, and Arg328 in the C1-subdomain (Figure 2B); therefore, Pi bridges these domains. In the ADP-Mg^{2+}-L-Ala-bound structure, the omit map clearly showed that the bound L-Ala was extensively recognized by the YwfE protein (Figure 2D). Both the oxygen atoms of the bound L-Ala are involved in bidentate electrostatic interactions with the guanidinium group of the side chain of Arg328, and one of the oxygen atoms is hydrogen bonded with the main-chain amide group of Gly331. The nitrogen atom of L-Ala has electrostatic interactions with the side chains of Glu273, His309, and Glu311. In addition, His309 makes van der Waals contacts with carbon and oxygen atoms of L-Ala. These residues are highly conserved among Lal, suggesting an important role in catalysis. The Cβ atom of L-Ala makes van der Waals contacts with Glu273, Trp332, and Met324. It is likely that these three residues determine the substrate specificity of YwfE for amino acid with the small side chain in the N-terminal substrate-binding pocket.

Functional Analysis by Site-Directed Mutations. It has been reported that YwfE prefers L-Ala for the N-terminal end and hydrophobic L-Phe or L-Met for the C-terminal end.[5,14] In the functional assay, we used the full-length YwfE (Met1−Val472) protein, and ATPase activity was measured in the combination of L-Ala and L-Phe or L-Met. For the wild-type enzyme, the ATPase activities increased with increasing concentrations of each amino acid, and the obtained curves were well fitted with the Michaelis−Menten equation (Figure S2, Supporting Information). The apparent K_m and k_{cat} values for Ala (1.64 ± 0.45 mM and 9.32 ± 0.89 s^{-1}), Phe (5.23 ± 1.59 mM and 10.4 ± 1.19 s^{-1}), and Met (11.3 ± 2.69 mM and 8.77 ± 0.96 s^{-1}) are similar to those previously reported.[14] The presence of either L-Ala or L-Phe did not show any activity. The affinity for L-Ser was 15-fold lower compared with that of L-Ala, and total activity was decreased to approximately half, which confirms that L-Ala is a suitable substrate for the N-terminal end.

Furthermore, on the basis of the present crystal structure, mutational analysis was performed to elucidate the contribution of each amino acid residue to substrate recognition and catalysis. ATPase assays were performed using the full-length mutants YwfE (Met1−Val472), and the obtained kinetic

dx.doi.org/10.1021/bi500292b | Biochemistry 2014, 53, 2650−2660

Table 2. Effect of Mutations on ATPase Activity[a]

YwfE	k_{cat} (s^{-1}) for Ala	K_m (mM) for Ala	k_{cat}/K_m ($mM^{-1}s^{-1}$) for Ala	k_{cat} (s^{-1}) for Phe	K_m (mM) for Phe	k_{cat}/K_m ($mM^{-1}s^{-1}$) for Phe
wild-type	9.32 ± 0.89	1.64 ± 0.45	6.07 ± 1.80	10.4 ± 1.19	5.23 ± 1.59	2.13 ± 0.58
E109A	<0.01			<0.01		
E109D	3.19 ± 1.43	7.12 ± 3.19	0.48 ± 0.14	1.83 ± 0.20	2.28 ± 0.96	0.91 ± 0.39
E273A	ND[b]			ND		
E273D	0.52 ± 0.26	17.06 ± 9.37	0.03 ± 0.00	0.49 ± 0.11	7.71 ± 2.58	0.08 ± 0.05
H276A	6.63 ± 1.34	7.72 ± 1.87	0.90 ± 0.26	4.36 ± 0.66	8.50 ± 0.70	0.51 ± 0.05
H309A	ND			ND		
H309R	ND			ND		
E311A	ND			ND		
E311D	<0.01			<0.01		
R328A	ND			ND		
R328 K	ND			ND		
W332A	4.32 ± 0.39	2.12 ± 0.31	2.07 ± 0.26	4.83 ± 0.55	15.9 ± 2.35	0.31 ± 0.08
M334A	2.62 ± 1.16	2.96 ± 1.82	0.95 ± 0.17	2.33 ± 0.41	3.70 ± 1.12	0.65 ± 0.08

[a]Reactions were performed as described in the Experimental Procedures section. The kinetic parameters were determined by the varying concentrations of either L-Ala or L-Phe. All k_{cat} and K_m values are shown as the mean ± standard deviation of at least three independent experiments. [b]ND means not detectable.

parameters are listed in Table 2. The mutation of each Glu273, His309, Glu311, and Arg328 residue to Ala almost completely diminished the activity, which is consistent with the structure-based predictions. An E273D mutation partially restored the activity, whereas H309R, E311D, and R328K enzymes remained inactive despite the similar charge-conserved mutations. These findings indicate that His309, Glu311, and Arg328 are the crucial residues for catalysis. It appears that the side chains of His309 and Arg328 along with the main-chain amide group of Gly331 form an oxyanion hole to stabilize the phosphorylated intermediate during the reaction cycle. The enzyme with substitution of Glu109 by Ala showed no activity, whereas that with substitution by Asp reduced the activity by approximately 30% compared with that of the wild type. The carboxyl group of Glu109 forms a hydrogen bond with the Nε atom of Arg328 (Figure 2C and D). In addition, at the opposite side, the main-chain carbonyl group of Phe329 forms a hydrogen bond with Arg328. These observations suggest that each residue plays an important role in fixing the side chain of Arg328 in the optimal conformation for L-Ala binding and catalytic reaction. An H276A mutation largely decreased the apparent K_m value for L-Ala approximately 5-fold but exerted little influence on the apparent K_m value for L-Phe, suggesting that His276 can contribute to L-Ala recognition, although it does not directly contact L-Ala. Mutation of Trp332 to Ala caused a decrease in catalytic efficiency (k_{cat}/K_m) for both L-Ala and L-Phe compared with that by the wild type. In addition, M334A mutation decreased the activity approximately 3-fold but did not strongly affect the apparent K_m value for each amino acid. Although Met334 is located in contact with the side chain of bound L-Ala, it is unlikely that this residue is essential for L-Ala binding.

L-Ala-Independent ATPase Activity of Trp332 Mutants. The W332A mutant appeared to retain considerable ATPase activity even in the absence of L-Ala (Figure 3A). In contrast, the addition of L-Ala alone to the reaction mixture showed no activity. It suggests that the mutant could accept L-Phe as an N-terminal end and may produce an L-Phe-L-Phe dipeptide, albeit at an extremely low turnover rate. To investigate the details of the L-Ala-independent ATPase activity observed in this W332A mutant, we measured ATPase activity at varying concentrations of L-Phe or L-Met in the absence of L-Ala. The activity at 50 mM L-Phe alone increased to approximately 20% of that in the presence of both L-Ala and L-Phe (Figure 3B). This L-Ala-independent activity was reduced at lower concentrations of L-Phe. Surprisingly, the ATPase activity increased with increasing concentrations of L-Met to almost the same levels regardless of L-Ala. The activity curve did not fit the Michaelis−Menten equation in the absence of L-Ala but did so in the presence of L-Ala. This observation suggests that L-Met is bound within two distinct binding pockets with different affinities in the absence of L-Ala. It was difficult to determine the apparent K_m value of each affinity.

To confirm the formation of an L-Phe-L-Phe product catalyzed by the YwfE W332A mutant, we performed reverse-phase HPLC analysis on a C_{18} column. The W332A mutant (10 μg) was incubated with 50 mM L-Phe in the presence of 10 mM ATP and 10 mM $MgCl_2$, and the reaction product in 250 μL was identified using a reference standard of an authentic L-Phe-L-Phe (2.5 μmol). The HPLC analysis showed that the W332A mutant enzyme produced about 1.4 μmol of the L-Phe-L-Phe dipeptide (Figure 4A and B). If all of the ATP molecules in the reaction mixture were consumed in order to produce the dipeptide, 2.5 μmol of the dipeptide would be detected by the HPLC analysis. The peaks that appeared before elution by acetonitrile corresponded to ATP (or ADP) and L-Phe (Figure S3A and B, Supporting Information). When the reaction was performed in the absence of ATP, the dipeptide was not observed (Figure S3C, Supporting Information). Thus, substitution of Trp332 with Ala will alter the substrate specificity of YwfE to allow the binding of larger amino acids, such as L-Phe, in the N-terminal substrate-binding pocket, and catalyzes the formation of the L-Phe-L-Phe dipeptide.

Crystal Structure of the W332A Mutant. To elucidate the role of Trp332 and the effects of its mutation on the structure of the substrate-binding pocket, we determined the crystal structure of the YwfE mutant W332A (Lys4−Tyr468) with bound ADP, Mg^{2+}, and L-Ala at 2.3 Å resolution (Table 1). The overall structure of the mutant was similar to that of the wild type with an rmsd of 1.2 Å for all Cα atoms. In addition, the mutant binds ADP and two Mg^{2+} in the same mode as that observed in the wild type. These findings indicate that mutation does not influence the overall fold or the nucleotide binding property. However, a large cavity seems to appear in the

dx.doi.org/10.1021/bi500292b | Biochemistry 2014, 53, 2650−2660

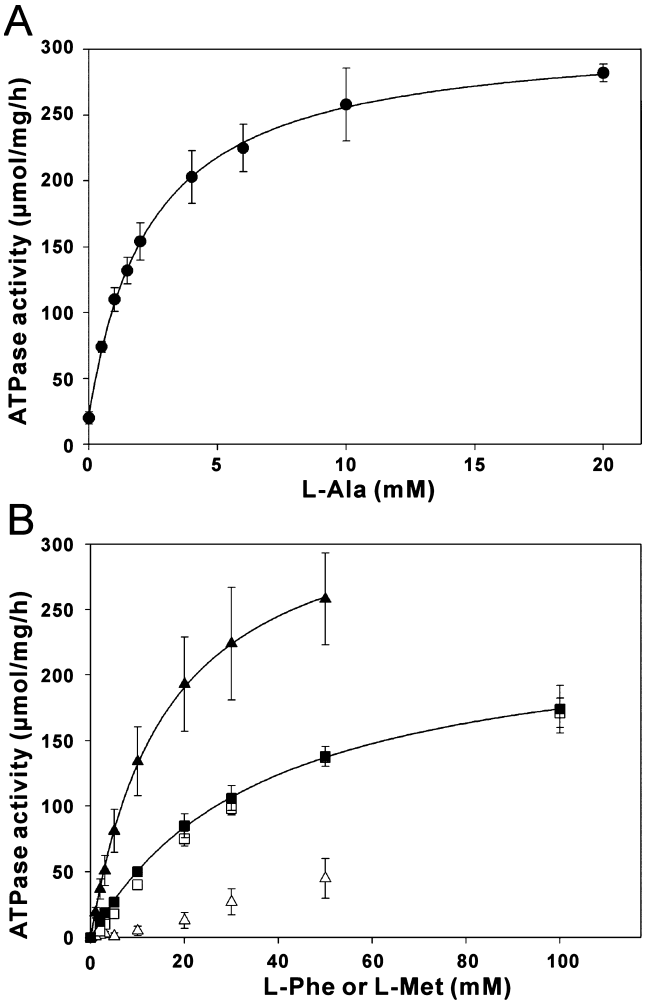

Figure 3. ATPase activity of W332A mutant. (A) The L-Ala concentration dependency of the ATPase activity of the W332A mutant was measured in the presence of 30 mM L-Phe (●). The curve was fitted to the Michaelis–Menten equation using the SigmaPlot software. The errors correspond to the standard deviation of at least three independent experiments. (B) The L-Phe (▲, △) or L-Met (■, □) concentration dependency of the ATPase activity was measured in the presence (closed symbols) or absence (open symbols) of 10 mM L-Ala. The curves could be fitted to a Michaelis–Menten equation when the measurements were performed in the presence of both L-Ala and L-Phe or L-Met.

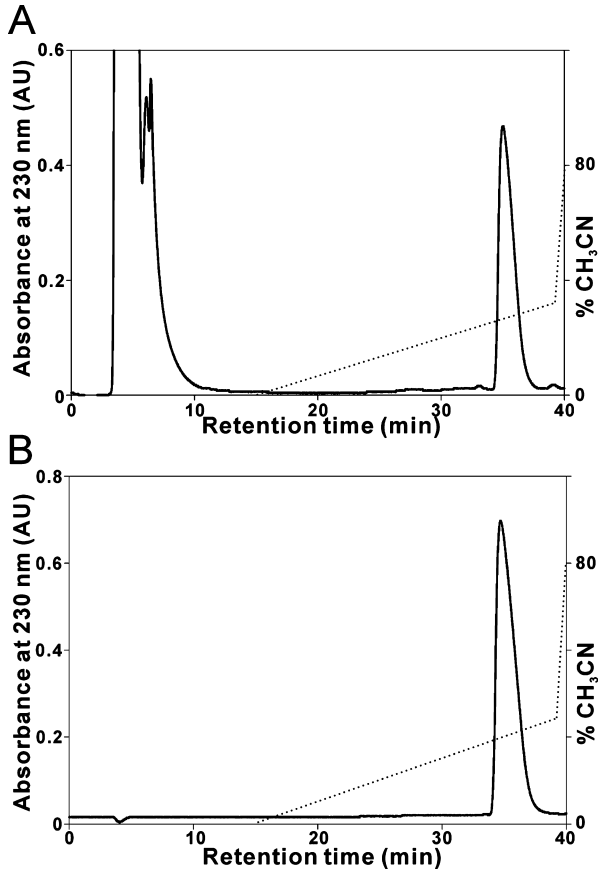

Figure 4. HPLC chromatograms. (A) 250 μL of the reaction products of the W332A mutant were separated by HPLC. The absorbance was monitored at 230 nm (left axis). The dotted lines indicate a linear gradient of acetonitrile (right axis). (B) An L-Phe-L-Phe standard (2.5 μmol) was separated by HPLC under the same conditions. The peak area values of the enzymatic reaction (A) and the standard (B) were estimated to be 38.23 AU × s and 66.56 AU × s, respectively, by using Clarify Lite software (DataApex).

mutant, due to the absence of the large indole ring of Trp332 (Figure 5A). This cavity is formed by the side chains of amino acid residues not only on the C1-subdomain (His276, Ala332, and Met334) but also on the C2-subdomain (Asp376, His378, and Tyr380). A Fourier difference ($|F_{obs}| - |F_{calc}|$) map before the introduction of L-Ala into the atomic model showed that the L-Ala bound in the same mode as that observed in the wild type. The model shows a large space over the Cβ atom of bound L-Ala, suggesting that this space is large enough to accommodate a larger amino acid such as L-Met. Thus, the large and rigid indole ring of Trp332 appears to restrict the substrate specificity for smaller amino acids such as L-Ala in the N-terminal substrate-binding pocket. The orientation of His378 was rotated by approximately 90° compared with that of the wild-type structure. This is because the planar surface of Trp332 is almost parallel to the imidazole ring of His378 via stacking interactions in the wild type (Figure 5B).

The structural and functional properties of W332A mutant YwfE remind us of those of BL00235. The crystal structure of BL00235 with bound ADP-Ca^{2+} showed a large hydrophobic cavity within a putative N-terminal substrate-binding pocket that is formed by the side chains on both C1- and C2-subdomains[15] (Figure 5C). The substrate specificity of BL00235 is entirely different from that of YwfE. It prefers L-Met and L-Leu for the N-terminal end and small substrates such as L-Ala, L-Ser, L-Thr, and L-Cys for the C-terminal end. It can be assumed that introduction of a large residue, such as Trp, into the entrance of the cavity of BL00235 would alter the substrate specificity for small amino acids, as is the case for YwfE. We have not yet obtained the crystal structure of the L-Met-bound form of the W332A mutant, although crystals were obtained in the presence of 10 mM ADP, 10 mM Mg^{2+}, and 100 mM L-Met. In the mutant crystal, the electron density corresponding to the expected side chain portion of L-Met was extremely weak, suggesting that the side chain of L-Met was disordered and did not interact strongly with the enzyme. This result is probably because of the lower affinity of the mutated enzyme for L-Met than for L-Ala, as expected from the functional assay.

Effect on the Substrate Specificity of Mutations at Position 332. To determine whether the size and shape of

dx.doi.org/10.1021/bi500292b | *Biochemistry* 2014, 53, 2650–2660

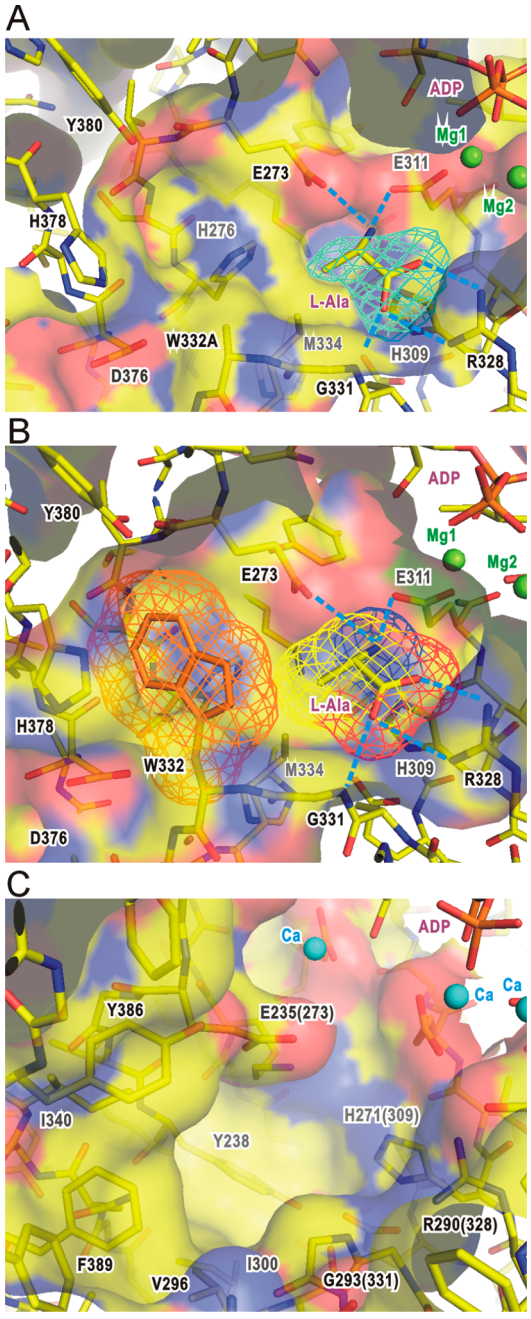

Figure 5. Molecular surface representation of the N-terminal substrate-binding site. (A) Structure of the W332A mutant of YwfE with bound ADP-Mg^{2+}-L-Ala. The cyan net represents a simulated omit map contoured at 3σ of L-Ala. (B) Structure of the wild-type YwfE with bound ADP-Mg^{2+}-Ala. The atom-type and orange nets represent van der Waals surfaces of bound L-Ala and the side chain of Trp332, respectively, in the wild-type ADP-Mg^{2+}-L-Ala-bound structure. (C) The structure of the expected N-terminal substrate-binding region of BL00235 with bound ADP-Ca^{2+} (PDB entry 3VOT). The numbers in parentheses represent the corresponding residues in YwfE.

amino acid residues at position 332 influence the L-Ala-independent ATPase activity, we prepared five additional Trp332 mutants, replacing Trp332 with Ser, Val, Leu, His, or Phe. First, we compared the effect of mutations on the ATPase activity under standard conditions (the presence of L-Ala and L-Phe). Substitutions of Trp332 with Ala, Ser, Val, Leu, or His decreased the activity approximately 70% to 40% compared with that of the wild type (black bars, Figure 6A). However,

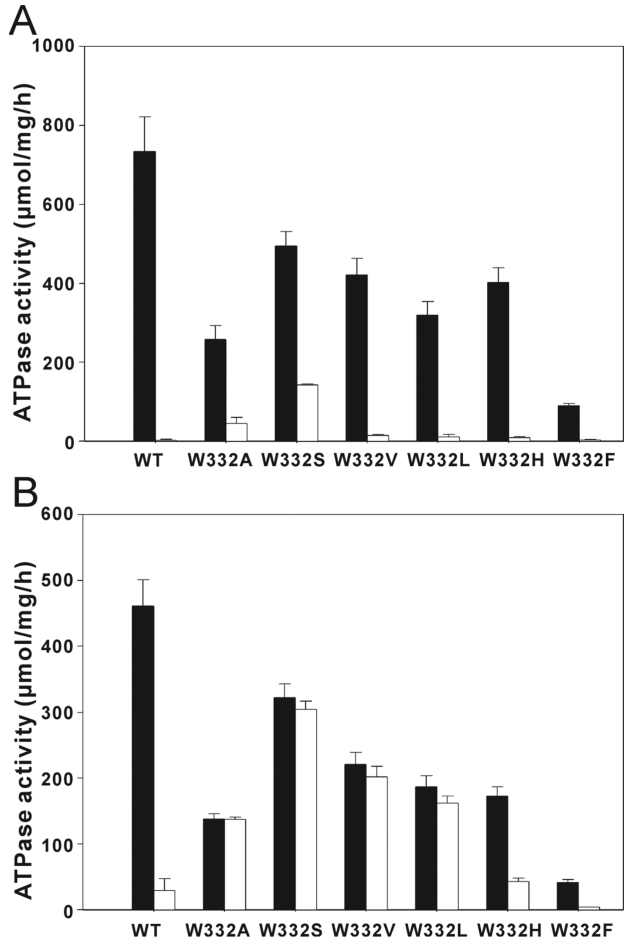

Figure 6. Effect of mutations at Trp332 on the L-Ala-independent ATPase activities. (A) The black and white bars represent 50 mM L-Phe-induced ATPase activities in the presence and absence of 10 mM L-Ala, respectively. The errors correspond to the standard deviations of at least three independent experiments. (B) The same measurements were performed except that 50 mM L-Met was used instead of L-Phe.

mutation of Trp332 to an aromatic Phe largely reduced the activity to >10% compared with that observed in the wild type. It is likely that a 6-member phenyl ring introduced at position 322 collides with the surrounding residues, such as Glu273 and His276, and influences the local structure within the substrate-binding pocket. When the same measurements were performed in the presence of L-Met instead of L-Phe, the results obtained were similar (black bars, Figure 6B). These findings indicate that the Trp residue at position 332 is not directly essential for the catalytic reaction.

Furthermore, to test each mutation on L-Ala-independent ATPase activity, the measurements were performed in the presence of 50 mM L-Phe or L-Met alone. Although the wild-type enzyme hardly showed any activity in the presence of 50 mM L-Phe alone, W332A and W332S retained activities of approximately 20% and 30%, respectively, compared with those in the presence of both L-Ala and L-Phe (white bars, Figure 6A). In contrast to these mutants, each mutant with substitution by Val, Leu, His, or Phe did not show any L-Ala-independent activity. When L-Met was used instead of L-Phe, even the wild-type enzyme retained approximately 6% of the L-Ala-dependent

dx.doi.org/10.1021/bi500292b | *Biochemistry* 2014, 53, 2650−2660

activity (white bars, Figure 6B). This result is consistent with the finding that YwfE has the ability to produce the L-Met-L-Met dipeptide.[5] In addition to W332A and W332S mutants, both W332V and W332L mutants also retained activities at almost the same levels, independent of the presence or absence of L-Ala. Furthermore, the enzyme with a mutation of Trp332 to His retained approximately 25% of the L-Ala-independent activity. These results indicate that each mutant prefers L-Met to the bulky and rigid L-Phe as a substrate. These functional and structural studies of Trp332 mutants allow us to propose that the size and shape of residues at position 332 of YwfE greatly influence substrate specificity in the N-terminal substrate-binding pocket.

Proposed Catalytic Mechanism. The reaction scheme of the ATP-grasp family is believed to proceed through the formation of an acylphosphate intermediate, which is attacked by a nucleophile, leading to a tetrahedral intermediate that ultimately collapses to form the product.[10,11] The superposition of the wild-type YwfE structure of ADP-Mg^{2+}-Pi and ADP-Mg^{2+}-L-Ala-bound forms demonstrated that one of the oxygen atoms from Pi was located very close to the position of the carboxyl oxygen from L-Ala (Figure 7). Thus, this model

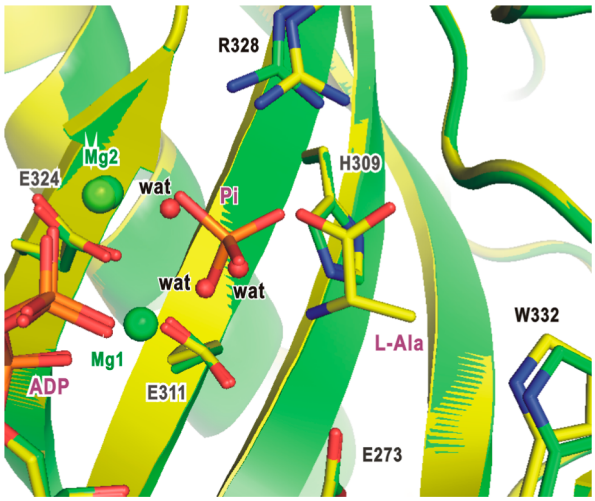

Figure 7. Model of an acylphosphate intermediate. Superimposition of models for the ADP-Mg^{2+}-L-Ala-bound form (atom color) and ADP-Mg^{2+}-Pi-bound form (green) of wild-type YwfE are shown. Side chains involved in important roles in the active site are presented as stick models. Three water molecules of the ADP-Mg^{2+}-L-Ala-bound structure are shown in red spheres.

appears to mimic the acylphosphate intermediate. In comparison with a P-analogue-bound model of YwfE, the acylphosphate portion in each model occupies a nearly identical position, suggesting that binding of phosphorylated L-Ala is firmly stabilized in the enzyme during the reaction cycle.

These considerations lead us to propose a scenario for the catalytic mechanism of YwfE enzyme. First, an ATP molecule is bound within the highly conserved nucleotide-binding cleft, and an L-Ala is recognized within the N-terminal substrate-binding pocket. Furthermore, Arg328 fixes the position of the carbonyl group of L-Ala to orient the positioning of one of the oxygen atoms and polarize a C−O bond suitable for the oxygen atom to attack the γ-phosphate group of ATP to produce an acylphosphate intermediate. An L-Phe (L-anticapsin *in vivo*) is subsequently bound within the C-terminal substrate-binding pocket, and its amino group makes a nucleophilic attack on the carbonyl carbon of the acylphosphate intermediate to form a tetrahedral transition state intermediate, which is stabilized by the positive charge environment formed with His309, Arg328, and the main-chain amide group of Gly331. Arg328 and the two Mg^{2+} ions assist the phosphate transfer and compensate the resulting negative charge in each intermediate. The phosphate is finally released from the acylphosphate to yield the L-Ala-L-Phe dipeptide (bacilysin *in vivo*), and ADP is also released from the nucleotide-binding site.

Role of Conserved Arg. In the catalysis and L-Ala recognition, the crucial residue appears to be Arg328. This Arg is conserved among the other members of the ATP-grasp enzymes. For example, the crystal structure of *E. coli* biotin-dependent carboxylase (BC) shows that bound bicarbonate is recognized by bidentate interactions with the side chain of Arg292.[30] The structure of *E. coli* PurK, one of the purine biosynthesis enzymes, in complex with ADP-Mg^{2+}-Pi, shows that conserved Arg242 recognizes the Pi molecule.[31] In the *E. coli* PurT structure, which is an enzyme participating in the purine biosynthetic pathway, Arg283 is located in the equivalent position to Arg242 in PurK.[32] In addition, the present study reveals that Arg328 plays an important role in the binding of L-Ala and Pi molecules. Amino acid sequence alignment with these enzymes indicates that the Mg1-coordinating Glu residue, which is also highly conserved in this family, is located four residues upstream from these Arg residues (Figure 8A). Although Ddl contains an Arg residue, which is crucial for D-Ala recognition and catalysis, this residue lies at a different position compared with those in other ATP-grasp enzymes. In *E. coli* DdlB,[33] Arg255 lies two residues downstream of another conserved Asp or Glu residue that coordinates Mg2. This Arg position is highly conserved among Ddl family members. YwfE and BL00235 contain important His residues, although the other members of the ATP-grasp superfamily carry uncharged residues at this position.

To compare the locations of the conserved Arg residues between Lal and Ddl, we superimposed the crystal structures of ADP-Mg^{2+}-L-Ala-bound YwfE and ADP-Mg^{2+}-D-Ala-bound Ddl from *Thermus thermophilus* HB8.[34] The structures were similar to an rmsd of 2.70 Å for structurally equivalent 255 Cα atoms. The model also showed that ADP and two Mg^{2+} occupy similar positions in each structure. As expected from the sequence alignment, the model clearly indicates that each Arg residue lies in a different position (Figure 8B). Both side chains of Arg328 in YwfE and Arg268 in TtDdl recognize each carboxyl group of bound L-Ala or D-Ala from the opposite side. As a result, the Ala molecules are bound by the enzyme in nearly reverse orientations. The different positioning of conserved Arg residues between Lal and Ddl will consequently cause the diverse orientation of the N- and C-terminal substrate-binding pockets in each enzyme. Despite the difference in the orientation of bound Ala, the two oxygen atoms of the carboxyl group of each Ala molecule exist in extremely similar positions. Superimposition of the structures of ADP-Mg^{2+}-Pi-bound YwfE and ADP-Mg^{2+}-phosphorylated phosphinate-bound *E. coli* DdlB[33] showed that the ADP, Mg^{2+}, and phosphate moieties in each structure occupied considerably similar positions (not shown). These observations suggest that the formation of an acylphosphate intermediate will occur in the same place independent of the different orientations of bound substrate amino acid. As mentioned above, L-Ala is strictly recognized by multiple electrostatic interactions with the side chains of Glu273, His309, Glu311, Arg328, and the

dx.doi.org/10.1021/bi500292b | *Biochemistry* 2014, 53, 2650−2660

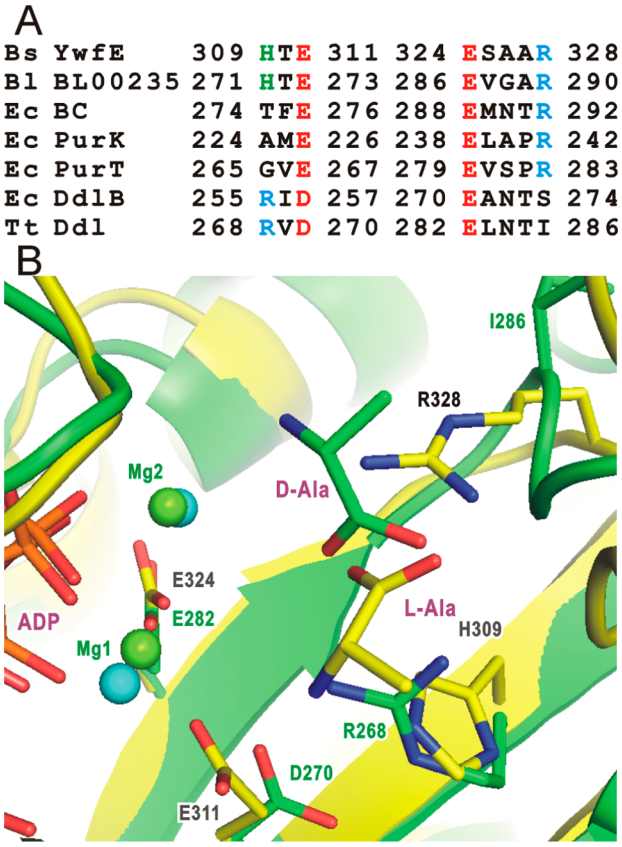

Figure 8. Conserved Arg residue in the ATP-grasp superfamily. (A) Bs, *Bacillus subtilis*; Bl, *Bacillus licheniformis*; Ec, *Escherichia coli*; Tt, *Thermus thermophilus* HB8. A structure-based sequence alignment of residues of conserved Arg (cyan), Mg^{2+}-coordinating Glu or Asp (red), and conserved His among only Lal (green) is shown. All residue numberings are shown on both sides of each line. (B) Superimposition of models for YwfE (atom color) and Ddl from *Thermus thermophilus* HB8 (green) with bound ADP-Mg^{2+}-L-Ala and ADP-Mg^{2+}-D-Ala, respectively. Mg^{2+} ions are represented by green (YwfE) and cyan (Ddl) spheres.

main-chain amide group of Gly321. Among these amino acids, the bidentate binding of the carboxyl group of L-Ala by Arg328 is important for the proper orientation of L-Ala. In addition, we propose that the different positioning of conserved Arg residues in Lal and Ddl is crucial for distinguishing the enantioselectivity in recognition of L- and D-amino acids.

Toward Rational Design of Lal. It has been proposed that Lals are potentially desirable tools for the enzymatic production of dipeptides composed of L-amino acids.[6] In the case of YwfE, an artificial sweetener aspartame (L-Asp-L-Phe-OMe) is likely to be a suitable and attractive candidate for a dipeptide that is produced by an engineered enzyme because L-Phe presents the highest affinity for the C-terminal substrate among the 20 proteogenic L-amino acids. However, restricted substrate specificity for smaller amino acids such as L-Ala at the N-terminus is one of the important issues that should be resolved for aspartame production. At present, the Trp332 mutant YwfE is a promising candidate for resolving this issue. We accordingly measured the ATPase activity of W332A mutant in the presence of L-Asp and L-Phe but observed that the activity was similar to that of the background, although L-Asp is smaller than L-Met or L-Phe. This result may be because of the negative charge of the side chain of L-Asp. To increase affinity and specificity for L-Asp, the introduction of a positively charged residue within the substrate-binding pocket of YwfE may be an effective strategy. One example of a successful change of substrate specificity was reported for subtilisin, a serine protease, in which electrostatic interactions between charged substrates and complementary charged amino acid residues in the substrate-binding pocket were engineered.[35] We are currently attempting to create a mutant YwfE with improved properties of substrate specificity and activity for L-Asp with the aim of engineering protein for the production of aspartame. Most recently, enzymatic production of L-Asp-L-Phe, a precursor of aspartame, by a two-step synthesis with a combination of Lal and yeast N-terminal amidase, given that no Lal has been identified that can produce a dipeptide carrying an acidic residue at the N terminus, has been reported.[36] In the first step, Lal catalyzed the formation of L-Asn-L-Phe from L-Asn and L-Phe, and subsequently, N-terminal amidase deamidated Asn to Asp to produce L-Asp-L-Phe. Several Lal's were identified in bacterial genomes by *in silico* screening, and each recombinant protein showed different substrate specificity. Detailed structural and functional studies of several other Lal's with bound amino acid substrates are desirable for elucidating the relationship between the substrate-binding pockets and amino acid substrate specificity. On the basis of this structural information, systematical introduction of point mutations, insertion, or deletion of amino acids in or near the substrate-binding pocket of Lal will allow the synthesis of modified Lal's with novel substrate-binding properties.

In conclusion, in this study, we determined new crystal structures of YwfE and performed mutagenesis studies. The results demonstrate that Trp332 plays a crucial role in restricting the substrate specificity for smaller amino acids such as L-Ala at the N-terminus and that a single mutation of YwfE can alter substrate specificity. To the best of our knowledge, this is the first demonstration of changing the substrate specificity of Lal by site-directed mutagenesis. These observations raise the possibility of engineering a suitable enzyme for the biosynthesis of dipeptides useful for industrial production. Taken together, our results provide useful guidelines for the rational design of Lal.

■ ASSOCIATED CONTENT

Supporting Information

Diffraction data statistics of Mn^{2+}-derivative crystals; orientation of Tyr75; ATPase activity of wild-type YwfE; and HPLC analysis. This material is available free of charge via the Internet at http://pubs.acs.org.

Accession Codes

The atomic coordinates and structure factors (codes 3WNZ, 3WO0, and 3WO1) have been deposited in the Protein Data Bank, Research Collaboratory for Structural Bioinformatics, Rutgers University, New Brunswick, NJ (http://wwwrscb.org/).

■ AUTHOR INFORMATION

Corresponding Author

*Tel: 83-3-3986-0221. Fax: 83-3-5992-1029. E-mail: takeo.tsuda@gakushuin.ac.jp.

Funding

This work was supported in part by a grant from JGC-S Scholarship Foundation to T.T.

Notes

The authors declare no competing financial interest.

■ ACKNOWLEDGMENTS

We would like to thank the beamline scientists at the Photon Factory for assistance with data collection. We thank Enago (www.enago.jp) for English language review.

■ ABBREVIATIONS

BC, biotin-dependent carboxylase; BSA, bovine serum albumin; Ddl, D-alanyl-D-alanine ligase; DTT, dithiothreitol; HPLC, high performance liquid chromatography; Lal, L-amino acid ligase; NRPS, nonribosomal peptide synthetase; PCR, polymerase chain reaction; PDB, protein data bank; PEG, poly(ethylene glycol); Pi, inorganic phosphate

■ REFERENCES

(1) Nolan, E. M., and Walsh, C. T. (2009) How nature morphs peptide scaffolds into antibiotics. *ChemBioChem. 10*, 34−53.
(2) Velasquez, J. E., and van der Donk, W. A. (2011) Genome mining for ribosomally synthesized natural products. *Curr. Opin. Chem. Biol. 15*, 11−21.
(3) Koglin, A., and Walsh, C. T. (2009) Structural insights into nonribosomal peptide enzymatic assembly lines. *Nat. Prod. Rep. 26*, 987−1000.
(4) Sieber, S. A., and Marahiel, M. A. (2005) Molecular mechanisms underlying nonribosomal peptide synthesis: approaches to new antibiotics. *Chem. Rev. 105*, 715−738.
(5) Tabata, K., Ikeda, H., and Hashimoto, S. (2005) *ywfE* in *Bacillus subtilis* codes for a novel enzyme, L-amino acid ligase. *J. Bacteriol. 187*, 5195−5202.
(6) Kino, K., Kotanaka, Y., Arai, T., and Yagasaki, M. (2009) A novel L-amino acid ligase from *Bacillus subtilis* NBRC3134, a microorganism producing peptide-antibiotic rhizocticin. *Biosci. Biotechnol. Biochem. 73*, 901−907.
(7) Kino, K., Arai, T., and Tateiwa, D. (2010) A novel L-amino acid ligase from *Bacillus subtilis* NBRC3134 catalyzed oligopeptide synthesis. *Biosci. Biotechnol. Biochem. 74*, 129−134.
(8) Senoo, A., Tabata, K., Yonetani, Y., and Yagasaki, M. (2010) Identification of novel L-amino acid α-ligases through Hidden Markov Model-based profile analysis. *Biosci. Biotechnol. Biochem. 74*, 415−418.
(9) Steinborn, G., Hajirezaei, M. R., and Hofemeister, J. (2005) *bac* genes for recombinant bacilysin and anticapsin production in *Bacillus* host strains. *Arch. Microbiol. 183*, 71−79.
(10) Galperin, M. Y., and Koonin, E. V. (1997) A diverse superfamily of enzymes with ATP-dependent carboxylate-amine/thiol ligase activity. *Protein Sci. 6*, 2639−2643.
(11) Fawaz, M. V., Topper, M. E., and Firestine, S. M. (2011) The ATP-grasp enzymes. *Bioorg. Chem. 39*, 185−191.
(12) Duerfahrt, T., Doekel, S., Sonke, T., Quaedflieg, P. J., and Marahiel, M. A. (2003) Construction of hybrid peptide synthetases for the production of α-L-aspartyl-L-phenylalanine, a precursor for the high-intensity sweetener aspartame. *Eur. J. Biochem. 270*, 4555−4563.
(13) Tabata, K., and Hashimoto, S. (2007) Fermentative production of L-alanyl-L-glutamine by a metabolically engineered *Escherichia coli* strain expressing L-amino acid α-ligase. *Appl. Environ. Microbiol. 73*, 6378−6385.
(14) Shomura, Y., Hinokuchi, E., Ikeda, H., Senoo, A., Takahashi, Y., Saito, J., Komori, H., Shibata, N., Yonetani, Y., and Higuchi, Y. (2012) Structural and enzymatic characterization of BacD, an L-amino acid dipeptide ligase from *Bacillus subtilis*. *Protein Sci. 21*, 707−716.
(15) Suzuki, M., Takahashi, Y., Noguchi, A., Arai, T., Yagasaki, M., Kino, K., and Saito, J. (2012) The structure of L-amino-acid ligase from *Bacillus licheniformis*. *Acta. Crystallogr., Sect. D 68*, 1535−1540.
(16) Tsuda, T., Suzuki, T., and Kojima, S. (2012) Crystallization and preliminary X-ray diffraction analysis of *Bacillus subtilis* YwfE, an L-amino-acid ligase. *Acta Crystallogr., Sect. F 68*, 203−206.
(17) Otwinowski, Z., and Minor, W. (1997) Processing of X-ray diffraction data collected in oscillation mode. *Methods Enzymol. 276*, 307−325.
(18) Ness, S. R., de Graaff, R. A., Abrahams, J. P., and Pannu, N. S. (2004) CRANK: new methods for automated macromolecular crystal structure solution. *Structure 12*, 1753−1761.
(19) Collaborative Computational Project, N (1994) The CCP4 suite: programs for protein crystallography. *Acta Crystallogr., Sect. D 50*, 760−763.
(20) Lamzin, V. S., and Wilson, K. S. (1993) Automated refinement of protein models. *Acta Crystallogr., Sect. D 49*, 129−147.
(21) Emsley, P., and Cowtan, K. (2004) Coot: model-building tools for molecular graphics. *Acta Crystallogr., Sect. D 60*, 2126−2132.
(22) Brünger, A. T., Adams, P. D., Clore, G. M., DeLano, W. L., Gros, P., Grosse-Kunstleve, R. W., Jiang, J. S., Kuszewski, J., Nilges, M., Pannu, N. S., Read, R. J., Rice, L. M., Simonson, T., and Warren, G. L. (1998) Crystallography & NMR system: A new software suite for macromolecular structure determination. *Acta Crystallogr., Sect. D 54*, 905−921.
(23) Winn, M. D., Murshudov, G. N., and Papiz, M. Z. (2003) Macromolecular TLS refinement in REFMAC at moderate resolutions. *Methods Enzymol. 374*, 300−321.
(24) Laskowski, R. A., MacArthur, M. W., Moss, D. S., and Thornton, J. M. (1993) PROCHECK: a program to check the stereochemical quality of protein structures. *J. Appl. Crystallogr. 26*, 283−291.
(25) DeLano, W. (2002) *The PyMOL Molecular Graphics System*; DeLano Scientific: Palo Alto, CA..
(26) Fiske, C. H., and Subbarow, Y. (1925) The colorimetric determination of phosphorus. *J. Biol. Chem. 66*, 375−400.
(27) Polekhina, G., Board, P. G., Gali, R. R., Rossjohn, J., and Parker, M. W. (1999) Molecular basis of glutathione synthetase deficiency and a rare gene permutation event. *EMBO J. 18*, 3204−3213.
(28) Gogos, A., and Shapiro, L. (2002) Large conformational changes in the catalytic cycle of glutathione synthase. *Structure 10*, 1669−1676.
(29) Fyfe, P. K., Alphey, M. S., and Hunter, W. N. (2010) Structure of *Trypanosoma brucei* glutathione synthetase: domain and loop alterations in the catalytic cycle of a highly conserved enzyme. *Mol. Biochem. Parasitol. 170*, 93−99.
(30) Chou, C. Y., Yu, L. P., and Tong, L. (2009) Crystal structure of biotin carboxylase in complex with substrates and implications for its catalytic mechanism. *J. Biol. Chem. 284*, 11690−11697.
(31) Thoden, J. B., Holden, H. M., and Firestine, S. M. (2008) Structural analysis of the active site geometry of N^5-Carboxyaminoimidazole ribonucleotide synthetase from *Escherichia coli*. *Biochemistry 47*, 13346−13353.
(32) Thoden, J. B., Firestine, S., Nixon, A., Benkovic, S. J., and Holden, H. M. (2000) Molecular structure of *Escherichia coli* PurT-encoded glycinamide ribonucleotide transformylase. *Biochemistry 39*, 8791−8802.
(33) Fan, C., Moews, P. C., Walsh, C. T., and Knox, J. R. (1994) Vancomycin resistance: structure of D-alanine: D-alanine ligase at 2.3 Å resolution. *Science 266*, 439−443.
(34) Kitamura, Y., Ebihara, A., Agari, Y., Shinkai, A., Hirotsu, K., and Kuramitsu, S. (2009) Structure of D-alanine-D-alanine ligase from *Thermus thermophilus* HB8: cumulative conformational change and enzyme-ligand interactions. *Acta Crystallogr., Sect. D 65*, 1098−1106.
(35) Wells, J. A., Powers, D. B., Bott, R. R., Graycar, T. P., and Estell, D. A. (1987) Designing substrate specificity by protein engineering of electrostatic interactions. *Proc. Natl. Acad. Sci. U S A 84*, 1219−1223.
(36) Arai, T., Noguchi, A., Takano, E., and Kino, K. (2013) Application of protein N-terminal amidase in enzymatic synthesis of dipeptides containing acidic amino acids specifically at the N-terminus. *J. Biosci. Bioeng. 115*, 382−387.